Integrated telecom wavelength heralded single-photon source based on Ghz gated detectors

De Matos Afonso Pereira, Maria Ana; Wu, Mingsong; Raja, A. S.; Wang, R. N.; Kippenberg, T.; Zbinden, Hugo; Brydges, Tiff; Thew, Rob

How to cite

DE MATOS AFONSO PEREIRA, Maria Ana et al. Integrated telecom wavelength heralded single-photon source based on Ghz gated detectors. In: Applied physics letters, 2026, vol. 128, n° 6, p. 064002. doi: 10.1063/5.0305411

This publication URL: https://archive-ouverte.unige.ch/unige:191426

Publication DOI: 10.1063/5.0305411

Applied Physics Letters

RESEARCH ARTICLE | FEBRUARY 11 2026

Integrated telecom wavelength heralded single-photon source based on GHz gated detectors

M. A. Pereira ; M. Wu ; A. S. Raja; R. N. Wang; T. Kippenberg; H. Zbinden ; T. Brydges ; R. Thew

Appl. Phys. Lett. 128, 064002 (2026)
https://doi.org/10.1063/5.0305411

Applied Physics Letters ARTICLE pubs.aip.org/aip/apl

Integrated telecom wavelength heralded single-photon source based on GHz gated detectors

Cite as: Appl. Phys. Lett. **128**, 064002 (2026); doi: 10.1063/5.0305411
Submitted: 6 October 2025 · Accepted: 17 January 2026 ·
Published Online: 11 February 2026

M. A. Pereira,[1] M. Wu,[1] A. S. Raja,[2] R. N. Wang,[2] T. Kippenberg,[2] H. Zbinden,[1,3] T. Brydges,[1] and R. Thew[1,a)]

AFFILIATIONS

[1]Department of Applied Physics, University of Geneva, Geneva, Switzerland
[2]Laboratory of Photonics and Quantum Measurements, EPFL, Lausanne, Switzerland
[3]Vigo Quantum Communication Center, Universidade de Vigo, Vigo E-36310, Spain

[a)]**Author to whom correspondence should be addressed:** robert.thew@unige.ch

ABSTRACT

We introduce a simple and flexible concept for a heralded—spectrally pure—single-photon source. The scheme uses a probabilistic photon-pair source pumped with a continuous-wave laser, whereby a rapid gating InGaAs/InP single-photon avalanche diode provides a synchronous clock for the system. The low timing jitter of the detector temporally resolves, and hence spectrally filters, the heralded photons. We demonstrate the concept by combining this with a narrow-band integrated silicon nitride photon-pair source. This simple architecture is capable of heralding photons with high spectral purity in the telecom band but could be adapted to other wavelengths and bandwidth regimes.

At the heart of all quantum photonic applications are technologies to generate and detect photons.[1] Historically, this has been dominated by probabilistic sources based on spontaneous parametric downconversion (SPDC) to generate entangled photons and semiconductor single-photon avalanche detectors (SPADs)—silicon for the visible regime and InGaAs/InP for telecom. In the last few years, this hegemony has been challenged by progress on the one hand in quantum dots,[2,3] whose performance is now surpassing that of probabilistic-based approaches such as SPDC, and on the other hand, the enormous advances in the performance of superconducting nanowire single-photon detectors (SNSPDs).[4]

Nonetheless, SPDC schemes and, more recently, spontaneous four-wave mixing (SFWM) can be readily engineered for a wide variety of wavelengths and bandwidths and can thus be adapted to suit a more diverse range of application scenarios. Along with SPADs, they also have the advantage of operating at room temperature or with simple electrical temperature control. SPADs can also be operated in different detection regimes—synchronous "gated" or asynchronous "free-running"—as required. A particularly interesting gated-mode regime in the telecom (InGaAs/InP) band involves rapidly gating the SPAD with short, sub-ns gates. This has advantages in terms of reduced noise (per gate) and afterpulsing, as well as having a lower detection jitter.[5]

SPDC and SFWM produce time-correlated photon pairs, whereby the detection of one photon of the pair can be used to herald the other, giving rise to the name heralded single-photon source (HSPS). Variations of HSPS using synchronous or asynchronous gated detectors have been demonstrated, where synchronized schemes have also relied on pulsed or modulated pump lasers, often adding to the complexity and cost of the scheme. Typically, these have only produced pure (spectrally uncorrelated) photons with careful phase matching and pump bandwidth engineering.[6]

In this work, an SFWM source is pumped with a continuous-wave (CW) laser, and, as such, the photon pairs can be generated at any time. However, as the detector's temporal resolution is much shorter than the photons' coherence time, the heralding detection projects the heralded photon into a well-defined single-mode temporal mode with high spectral purity. In parallel, the gating of the detectors provides a simple means of translating the CW-pumped SPDC source into a synchronous stream of heralded photons. This simple approach to HSPS can be easily adapted to other photonic sources, provided that

the photon coherence length is longer than the jitter of the detector.[7] Indeed, the concept of temporally resolved detections has previously been exploited to enable entanglement swapping experiments between CW sources.[8,9] In the following, we first explain how the SPAD functions, then describe the photon-pair source, showing their characterizations, before elaborating on the HSPS concept and presenting the results.

Near-infrared (NIR) free-running single-photon detectors are essential for a number of applications, such as LiDAR and biomedical sensing.[10–14] Among the leading single-photon detector technologies are superconducting nanowire single-photon detectors (SNSPDs) that offer exceptional performance with near-unity detection efficiency and ultra-low dark counts. However, SNSPDs rely on cryogenic cooling, which significantly increases their complexity and limits their suitability for some applications. By contrast, InGaAs/InP single-photon avalanche diodes (SPADs) are widely used for NIR detection due to their simplicity, low cost, low power consumption, and small footprint. For high-speed performance, gated-mode SPADs are preferred—often referred to as rapid gating. The small active time of the gated signal ensures low timing jitters as well as lower dark count rates (DCRs) and afterpulsing effects when compared to free-running or standard gated SPADs.[5,15–18] The afterpulse probability (P_{ap}) is a limiting factor for the maximum count rates in SPADs, as it generally requires long hold-off times (time after an avalanche event during which the detector is kept below its breakdown voltage) to be suppressed.

When InGaAs/InP SPADs are used in gated mode, the output signal of a typical SPAD includes the avalanche signal (a few millivolts) and a strong parasitic signal that can be orders of magnitude higher than the avalanche signal. This parasitic signal is a capacitance response (CR) caused by the rapid change in voltage across the SPAD when a gate is applied and is proportional to both the capacitance and the rate of voltage change. There are two obvious ways of detecting single-photon events in these conditions: either the bias of the detectors is increased in order to have larger avalanches that can be easily discriminated from the CR—resulting in a higher dark count rate (DCR) and afterpulsing probability (P_{ap})—or complex readout electronics are used to reduce the CR. The first approach of increasing the bias voltage creates a problematic feedback loop: higher bias leads to more intense avalanche events, which trap more charge carriers in defects, increasing P_{ap}. To mitigate this, longer hold-off times are required, which in turn limits the maximum achievable count rate.

An alternative approach to this takes a copy of the signal, delays it by one period, and then subtracts the signals to eliminate this CR.[19] An extension of this concept introduced a second SPAD to provide a reference signal that could be subtracted instead.[20] Park *et al.*[21] took this a step further and developed dual-anode InGaAs/InP SPADs (DA-SPADs) that are comprised of two on-chip diodes separated by an isolation wall and sharing a common cathode. Both diodes are designed to operate as SPADs; however, one diode serves as a *dummy* and is engineered to have a higher breakdown voltage compared to the other diode, which makes it unable to detect single photons. In principle, the *dummy* detector creates a CR similar to that of the main detector, which is later removed from the detection's output signal via a subtraction circuit. This enables the detection of smaller avalanche signals that would otherwise be hidden by the CR, allowing for a better discrimination and readout efficiency of the detection signal, while keeping DCR and P_{ap} relatively low.

Figure 1 is a schematic representation of the experimental setup used for characterizing the detector's (WOORIRO, SPAD with internal TEC) photon detection efficiency (PDE), DCR, and P_{ap} using an attenuated laser. A pulsed laser at 1550 nm was connected to a variable optical attenuator, reducing the mean photon number per pulse to 0.5. The electrical part of the experimental setup comprises a sine generator, used for the gate generation, sent to an RF amplifier followed by a low-pass filter, before being sent to the detector. A source meter was used to supply the required DC voltage to the detector, which was subsequently connected to a subtracting circuit. External to the detector's control PCB, the output signal was then discriminated, and the TTL signal was sent to a time tagger [ID Quantique, ID900]. The time tagger also acted as a reference clock for the characterization setup, providing a 10 MHz clock signal to the sine generator and a periodic trigger signal to a pulsed laser used for characterization. The detector was gated at 1 GHz, using a sine wave with 20 V_{pp}, and an effective gate width below 300 ps.

To accurately measure the PDE, the laser repetition rate (f_L) was set to 100 kHz and synchronized with the detector gating. This low repetition rate provides enough time between laser pulses, preventing afterpulsing events from artificially inflating the PDE. The characterization of PDE, DCR, and P_{ap} was then performed by collecting a single histogram spanning the totality of the pulsed laser's period (10 μs), with bin widths as to include one gate/bin (1 ns), corresponding to the 1 GHz gate frequency.

Traditionally, the PDE is calculated using the expression

$$\mathrm{PDE} = \frac{1}{\mu}\ln\left(\frac{1-P_d}{1-P_t}\right), \tag{1}$$

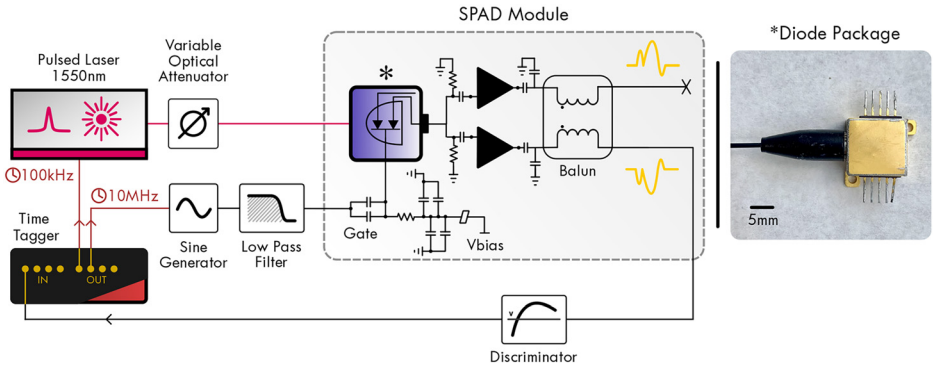

FIG. 1. Schematic of the setup used for characterizing the SPAD, along with a picture of the diode package.

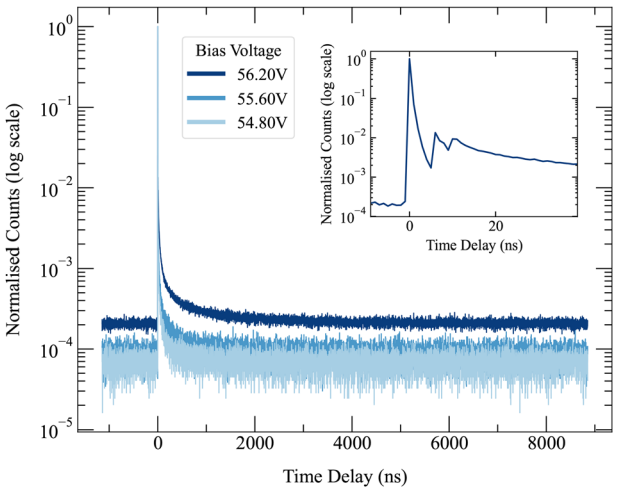

FIG. 2. Detection count histograms (normalized to the maximum) showing the time delay distribution of afterpulsing and dark count events relative to laser pulse events, which is defined to be at 0 ns delay. Data collected at different SPAD bias voltages are shown to illustrate the increase in afterpulsing occurrence and dark count rate with bias voltage. Inset: Data for a bias voltage of 56.20 V, shown near 0 ns. The integration time was 120 s.

where P_d and P_t are the dark count probability and total count probability, respectively, and μ is the mean photon number per laser pulse. The natural logarithmic terms are Poissonian corrections when converting between detection probabilities and detection rates.[22] Since our setup allowed access to all the key parameters directly, we used an alternative method to calculate the PDE. Figure 2 depicts sample data representing the temporal distribution of afterpulsing/dark count events occurring after each laser pulse. The characterization used short laser pulses, <50 ps full width at half maximum (FWHM), that were aligned in time such that they were completely contained in a single histogram bin, with bin-width $\Delta t = 1$ ns. As seen in the plot inset, after the initial laser irradiation peak, a sharp decrease in counts in the subsequent 10 ns was observed. This behavior emerges from the discriminator's inherent dead time, caused by the bandwidth limitations of its monostable circuit (see the supplementary material).

The PDE can then be directly calculated from the signal counts in the time bin corresponding to the arrival of the laser pulse while correcting for dark counts

$$\mathrm{PDE} = \frac{C_L - DCR \times \Delta t}{\mu' \times N_L}, \tag{2}$$

where C_L represents the total counts in the signal bin, Δt the histogram's bin width, and N_L is the total number of pulses. A corrected mean photon number per pulse, μ', is defined by

$$\mu' = 1 - \left.\frac{\mu^n e^{-\mu}}{n!}\right|_{n=0} = 1 - e^{-\mu}. \tag{3}$$

This represents the Poissonian correction to the mean photon number (μ), calculated using an average optical power measurement to obtain the probability of having *at least* one photon per pulse. Finally, the DCR can be calculated either by measuring the histogram with the laser off or by only considering the counts at very large time delays.

The P_{ap} can be characterized by physically implementing different hold-off times in the discrimination circuit. However, this would require multiple dataset measurements and also requires physical modifications to the discriminator hardware between each measurement. Here, the P_{ap} was calculated for various arbitrary set hold-off times (t_d) through post-processing by discarding the counts in the t_d bins following the laser-illuminated bin from the histogram.

The P_{ap} is then given by the ratio of counts due to afterpulsing (total non-illuminated counts collected on histogram) and illuminated counts, both corrected for DCR

$$P_{ap} = \frac{C_T - C_L - DCR \times \Delta T}{C_L - DCR \times \Delta t}, \tag{4}$$

where C_T refers to the total counts for a chosen hold-off time t_d, ΔT is the corresponding integration time, and C_L is the total counts in the signal bin. Importantly, this approach achieves the same result as physically implementing different hold-off times in the discriminator circuit but requires only one histogram for all analyses and eliminates the need to modify the discriminator hardware.

The discriminator threshold level, V_{th}, can have a profound effect on the performance of the detector. V_{th} should be set as low as possible to catch all small avalanches from photon events to improve the signal readout efficiency. However, due to imperfections in the detector and associated electronic components, the measured signal is distorted in the gates before and after an avalanche signal. As such, a compromise has to be made on the efficiency to avoid picking up these noisy readout signals. Figure 3 shows the calculated efficiency from Eq. (2) as a function of dark count probability per gate for various discrimination threshold settings, where we obtained the best PDE-to-noise performance with $V_{th} = -243.0$ mV, as well as settings with higher and lower voltage thresholds to illustrate their reduced performance. A corresponding curve using Eq. (1) to calculate the PDE is also shown for comparison: We saw generally good agreement, with Eq. (1) giving a

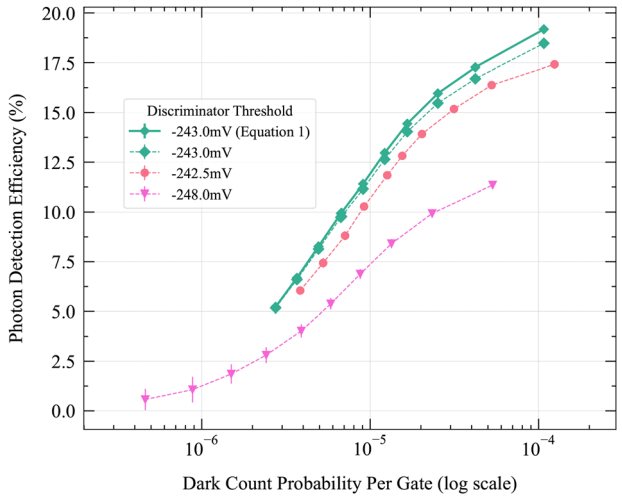

FIG. 3. Characterization data of the SPAD detector, where corresponding dark count probability per gate and photon detection efficiencies (PDEs) are shown against varying discriminator threshold values. Dashed lines show the PDE calculated from Eq. (2), with the solid line showing the PDE calculated from Eq. (1). The PDE is adjusted by changing the SPAD bias voltage.

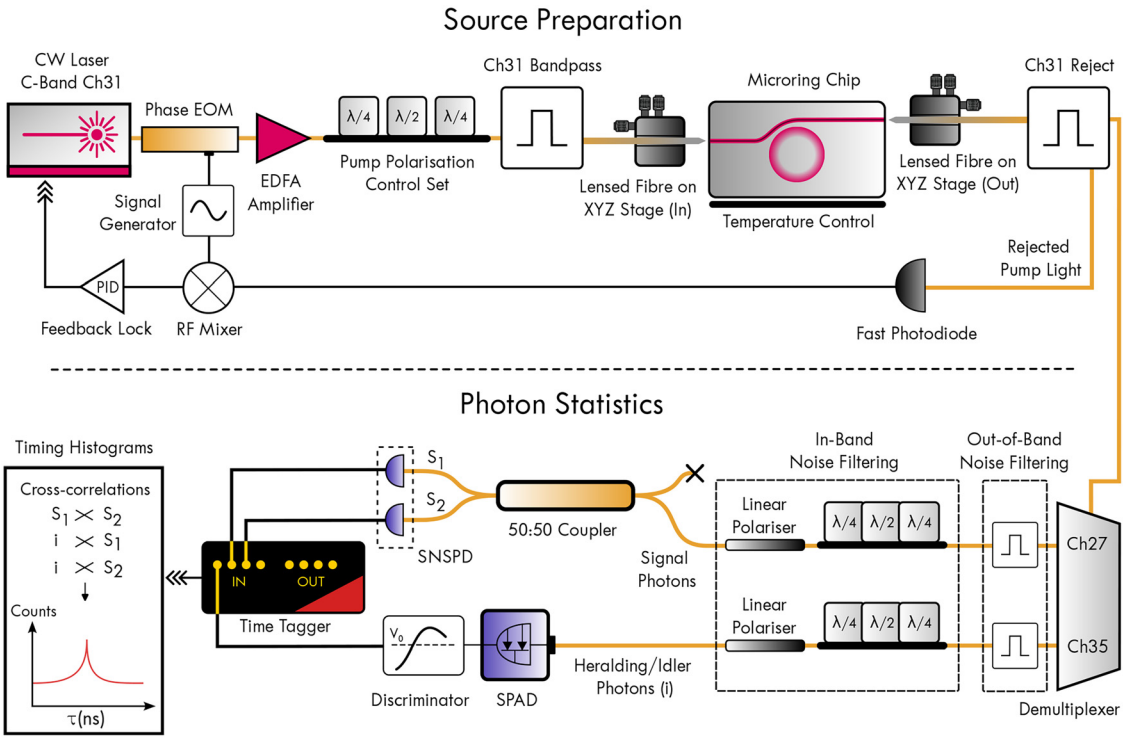

FIG. 4. Schematic of the experimental setup, starting with the photon-pair source preparation stage followed by the photon statistics stage. The former concerns the generation of photon pairs by coupling laser light into the microring and locking the pump frequency to a resonant mode of the microring. The latter filters out residual pump light and frequency demultiplexes the photon pairs for detection in a (heralded) HBT setup.

slightly higher PDE. While this does not affect the performance of the HSPS characteristics, further work is required to better understand this small discrepancy. For the following measurements, we chose a PDE working point of 15.5%, which was chosen after performing a parameter sweep of detector bias voltage and discriminator values while measuring the PDE, DCR, and P_{ap}.

Finally, the jitter was characterized from measurements obtained using a similar time-tagging setup in Fig. 1. Under the same PDE conditions, we measured the upper bound for the FWHM jitter to be 30 ps, significantly shorter than for typical SPADs, where jitter usually exceeds 100 ps.[23,24] Measurement data and setup details may be found in the supplementary material.

A key component of the fully fiber-based heralded single-photon source (HSPS) presented here was the microring resonator (MRR) photon-pair source, based on a silicon nitride integrated photonic chip. Telecom wavelength photon pairs (signal-idler) were generated via SFWM. These pairs were out-coupled and frequency demultiplexed using dense wavelength-division multiplexing (DWDM) filters, with the idler photons detected as heralds for the signal photons. The integrated fiber-based design allowed the setup to be highly compact and robust. Figure 4 shows a schematic of the full experimental setup. The MRR had a 200 GHz free spectral range and was pumped at 1552.5 nm with light from a CW laser (<5 MHz linewidth). For further details on the source, see the supplementary material.

The MRR chip temperature was actively stabilized, and the Pound–Drever–Hall (PDH) technique[25] was used to actively lock the laser frequency to the cavity resonance using a Red Pitaya and home-built amplifier board. The device had Q-factors for pump, signal, and idler on the order of 3.5×10^6, corresponding to signal (idler) bandwidths of about 53 MHz (60 MHz).

To quantify the performance of the HSPS, we look at both the single-photon and spectral purity of the source. To characterize the single-photon purity of the HSPS, the heralded autocorrelation, $g_h^{(2)}(0)$, was measured using the experimental setup shown in Fig. 4. A value of 0.198 ± 0.005 was obtained for an MRR chip input power of 235 μW, an integration time of 7752 s, and a coincidence window of 3 ns. This pump power corresponds to a photon-pair probability of $\sim 0.2\%$ per gate and $\sim 3\%$ per coherence time. The SPAD settings are given in Table I and the photon-pair source parameters are given in Table II.

The spectral purity is quantified by measuring the unheralded second-order correlation function, $g_{auto}^{(2)}(\tau)$, shown in Fig. 5.[26] To do this, one of the SNSPDs on the heralded arm is replaced with the

TABLE I. Detector parameters for characterizing the HSPS, with a fixed gating frequency of 1 GHz. P_{DC} is the dark count probability per gate.

PDE (%)	P_{DC}	V_{th} (mV)	t_d (μs)	P_{ap} (%)	Gate width (ps)
15.5	1.25×10^{-5}	−243	5	< 1.0	<300

TABLE II. Photon-pair source parameters for characterizing the HSPS, with the pump power at chip input being 660 μW. η_{coup} is the average coupling efficiency, with PGR the pair generation rate (see the supplementary material).

$\Delta\nu_s$ [$\Delta\nu_i$] (MHz)	η_{coup} (%)	PGR (MHz)	$g^{(2)}_{auto}(0)$
52.8 [59.8]	~44	~ 7.5	1.98(1)

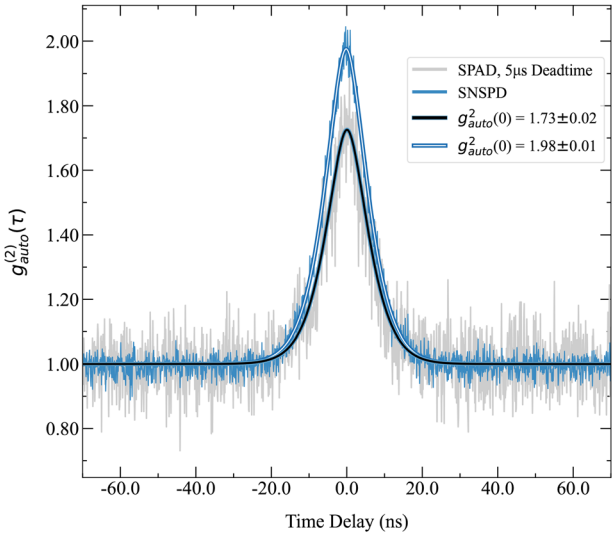

FIG. 5. Autocorrelation measurement of the signal photon stream using an SNSPD and either our SPAD or another SNSPD, as well as the data fits.[26] The SPAD had a software-level 5 μs dead time applied to the time tags to filter afterpulsing events.

SPAD in Fig. 4. The $g^{(2)}_{auto}(0)$ can be straightforwardly related to the photon's spectral purity[27] via $P = g^{(2)}_{auto}(0) - 1$, with the HSPS having a spectral purity of $P = 0.73 \pm 0.02$. For comparison, also shown is the result from a measurement performed using two SNSPDs, yielding $g^{(2)}_{auto}(0) = 1.98 \pm 0.01$ ($P = 0.98 \pm 0.01$), indicating the MRR itself produces photon pairs with very high spectral purity. The reduction in spectral purity when using the SPAD as the heralding detector can be mainly attributed to a higher DCR, as the $g^{(2)}_{auto}(0)$ is not dependent on the detector efficiency, and the jitter of the two types of detectors is comparable.

An important quantity to characterize the performance of an HSPS is the heralding efficiency—the probability of the heralded photon being in the output mode, $\eta_{h,s}$. To calculate this, the coincidence count rate $R_{s,i}$ within a coherence time of the signal and idler photons was first determined from

$$R_{s,i} = \frac{1}{\Delta T} \sum_{\tau > -\tau_{c,s}}^{\tau < \tau_{c,i}} C_\tau, \tag{5}$$

where the summation represents the total counts from time bins where τ is within the (asymmetric) photon coherence times $\tau_{c,s}$ and $\tau_{c,i}$ and ΔT is the integration time. $\tau_{c,s}$ and $\tau_{c,i}$ are extracted from the signal-idler cross correlation histogram (see the supplementary material). The signal photon heralding efficiency, $\eta_{h,s}$, can then be calculated from

$$\eta_{h,s} = \frac{R_{s,i}}{R_i \eta_{d,s}}, \tag{6}$$

where $\eta_{d,s}$ is the heralded (signal) detector PDE and R_i is the idler photon count rate measured on the SPAD.[28] The heralded signal photon count rate ($R_{h,s}$) follows as $\eta_{h,s}R_i$.

Figure 6 shows $\eta_{h,s}$ and the photon heralding rate for the 53 MHz bandwidth signal photons as functions of pump power. We observe the photon heralding efficiency increasing with pump power, which is linked to the relatively high DCR of the SPAD: As the photon-pair rate increases with a constant DCR, the probability of detecting a true (idler photon) heralding event per gate also increases with pump power. We ascribe the approximately linear behavior of this increasing trend to how the idler single-photon rates increase with pump power (see the supplementary material). A notable linear component is observed in the otherwise quadratic relationship of idler singles rate vs pump power due to the SPAD hold-off time, along with resonant Raman noise generated in the MRR. Additionally, the heralding efficiency is adversely affected by transmission losses through the channel between the MRR chip and detector; however, these losses can be improved with more optimized filtering. In this proof of concept demonstration we used 660 μW of pump power at the MRR chip, observing $\eta_{h,s} \sim 3.9\%$ and $R_{h,s} \sim 2.0$ kHz for photons with spectral bandwidths around 50 MHz.

This paper has shown the proof-of-principle demonstration of a telecom HSPS comprised of an integrated photon-pair source in combination with a dual-anode InGaAs/InP SPAD[21] operated at GHz gate rates. Due to the CW pumping of the source, the SPAD is not only used for single-photon detection but is also used as the synchronization signal for clocking the entire system. In this work, the SPAD was operated at a 1 GHz rate; however, detectors suitable for this scheme can be operated at much higher rates, in excess of 2 GHz.[5,16] Although the demonstration in this work used a very narrow-band source, the SPAD's low jitter would allow its use with photon bandwidths above even 20 GHz, while still allowing the detection of the heralding photon to project the heralded photon into a well-defined, synchronously clocked stream of photons,[7] depending on the desired application.

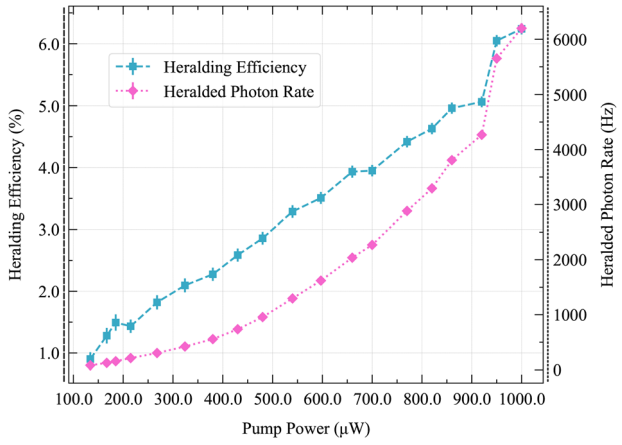

FIG. 6. The heralded signal photon rate and heralding efficiency as functions of pump power. Error bars are derived from the Poissonian error of the photon count rates.

Our HSPS setup is currently limited by the noise characteristics of the SPAD. This could be addressed through developing a more advanced detector control PCB to allow for adjustment of both phase and amplitude of each diode's CR within the subtraction circuit, which would suppress the background CR signal further and thus allow a better readout efficiency with substantially reduced DCR and P_{ap} for the same PDE. Ideally, though, this should also be addressed at the fabrication stage for the dual-anode InGaAs/InP SPADs. In principle, a dark count probability per gate on the order of 2×10^{-6} could then be reasonably expected,[5] leading to the predicted $g^{(2)}_{auto}(0)$ using an SPAD and an SNSPD potentially improving to $g^{(2)}_{auto}(0) = 1.95$, and when using two SPADs of $g^{(2)}_{auto}(0) = 1.90$.[29] The simple nature of the concept and all HSPS components in this work demonstrates the potential for future, improved HSPSs in field-deployed quantum networks.

See the supplementary material for technical specifications and experimental characterization details for the integrated HSPS and the GHz SPAD detector.

The authors thank Alberto Boaron and ID Quantique for the dual-anode InGaAs/InP SPAD. We acknowledge David Cabrerizo for assistance with the in-house electronics development. This work was supported by the Swiss State Secretariat for Research and Innovation (SERI) (Contract No. UeM019-3). T.B. and M.W. are supported by the Swiss National Science Foundation through Ambizione Grant No. PZ00P2_216153.

AUTHOR DECLARATIONS

Conflict of Interest

The authors have no conflicts to disclose.

Author Contributions

M. A. Pereira and M. Wu contributed equally to this paper.

M. A. Pereira: Conceptualization (equal); Data curation (equal); Formal analysis (equal); Investigation (equal); Methodology (equal); Project administration (equal); Resources (equal); Software (equal); Validation (equal); Visualization (equal); Writing – original draft (equal); Writing – review & editing (equal). **M. Wu:** Conceptualization (equal); Data curation (equal); Formal analysis (equal); Investigation (equal); Methodology (equal); Project administration (equal); Resources (equal); Software (equal); Validation (equal); Visualization (equal); Writing – original draft (equal); Writing – review & editing (equal). **A. S. Raja:** Conceptualization (supporting); Data curation (equal); Formal analysis (equal); Funding acquisition (supporting); Investigation (equal); Methodology (equal); Project administration (supporting); Resources (supporting); Software (equal); Supervision (equal); Validation (equal); Visualization (equal); Writing – original draft (supporting); Writing – review & editing (supporting). **R. N. Wang:** Conceptualization (supporting); Data curation (equal); Formal analysis (equal); Funding acquisition (supporting); Investigation (equal); Methodology (equal); Project administration (supporting); Resources (equal); Software (equal); Supervision (equal); Validation (equal); Visualization (equal); Writing – original draft (supporting); Writing – review & editing (supporting). **T. Kippenberg:** Conceptualization (equal); Data curation (equal); Formal analysis (equal); Funding acquisition (equal); Investigation (equal); Methodology (equal); Project administration (equal); Resources (supporting); Software (equal); Supervision (lead); Validation (equal); Visualization (equal); Writing – original draft (equal); Writing – review & editing (supporting). **H. Zbinden:** Conceptualization (equal); Data curation (equal); Formal analysis (equal); Funding acquisition (equal); Investigation (equal); Methodology (equal); Project administration (equal); Resources (equal); Software (equal); Supervision (lead); Validation (equal); Visualization (equal); Writing – original draft (equal); Writing – review & editing (supporting). **T. Brydges:** Conceptualization (lead); Data curation (equal); Formal analysis (lead); Funding acquisition (equal); Investigation (equal); Methodology (equal); Project administration (equal); Resources (equal); Software (equal); Supervision (lead); Validation (equal); Visualization (equal); Writing – original draft (equal); Writing – review & editing (equal). **R. Thew:** Conceptualization (equal); Data curation (equal); Formal analysis (equal); Funding acquisition (equal); Investigation (equal); Methodology (equal); Project administration (equal); Resources (equal); Software (equal); Supervision (equal); Validation (equal); Visualization (equal); Writing – original draft (equal); Writing – review & editing (equal).

DATA AVAILABILITY

The data that support the findings of this study are available from the corresponding author upon reasonable request.

REFERENCES

[1]M. D. Eisaman, J. Fan, A. Migdall, and S. V. Polyakov, "Invited review article: Single-photon sources and detectors," Rev. Sci. Instrum. **82**, 071101 (2011).
[2]N. Tomm, A. Javadi, N. O. Antoniadis, D. Najer, M. C. Löbl, A. R. Korsch, R. Schott, S. R. Valentin, A. D. Wieck, A. Ludwig, and R. J. Warburton, "A bright and fast source of coherent single photons," Nat. Nanotechnol. **16**, 399–403 (2021).
[3]X. Ding, Y.-P. Guo, M.-C. Xu, R.-Z. Liu, G.-Y. Zou, J.-Y. Zhao, Z.-X. Ge, Q.-H. Zhang, H.-L. Liu, L.-J. Wang, M.-C. Chen, H. Wang, Y.-M. He, Y.-H. Huo, C.-Y. Lu, and J.-W. Pan, "High-efficiency single-photon source above the loss-tolerant threshold for efficient linear optical quantum computing," Nat. Photonics **19**, 387–391 (2025).
[4]D. V. Morozov, A. Casaburi, and R. H. Hadfield, "Superconducting photon detectors," Contemp. Phys. **62**, 69–91 (2021).
[5]J. Zhang, P. Eraerds, N. Walenta, C. Barreiro, R. Thew, and H. Zbinden, "2.23 GHz gating InGaAs/InP single-photon avalanche diode for quantum key distribution," in *Advanced Photon Counting Techniques IV*, edited by M. A. Itzler and J. C. Campbell (International Society for Optics and Photonics, SPIE, 2010), Vol. 7681, p. 76810Z.
[6]P. J. Mosley, J. S. Lundeen, B. J. Smith, P. Wasylczyk, A. B. U'Ren, C. Silberhorn, and I. A. Walmsley, "Heralded generation of ultrafast single photons in pure quantum states," Phys. Rev. Lett. **100**, 133601 (2008).
[7]Y.-P. Huang, J. B. Altepeter, and P. Kumar, "Heralding single photons without spectral factorability," Phys. Rev. A **82**, 043826 (2010).
[8]M. Halder, A. Beveratos, N. Gisin, V. Scarani, C. Simon, and H. Zbinden, "Entangling independent photons by time measurement," Nat. Phys. **3**, 692–695 (2007).
[9]F. Samara, N. Maring, A. Martin, A. S. Raja, T. J. Kippenberg, H. Zbinden, and R. Thew, "Entanglement swapping between independent and asynchronous integrated photon-pair sources," Quantum Sci. Technol. **6**, 045024 (2021).
[10]C. Yu, J. Qiu, H. Xia, X. Dou, J. Zhang, and J.-W. Pan, "Compact and lightweight 1.5 μm lidar with a multi-mode fiber coupling free-running InGaAs/InP single-photon detector," Rev. Sci. Instrum. **89**, 103106 (2018).

[11]Y. Liang, B. Xu, Q. Fei, W. Wu, S. Xiao, K. Huang, and H. Zeng, "Low-timing-jitter GHz-gated InGaAs/InP single-photon avalanche photodiode for LIDAR," IEEE J. Sel. Top. Quantum Electron. **28**, 1–7 (2022).
[12]Z.-P. Li, J.-T. Ye, X. Huang, P.-Y. Jiang, Y. Cao, Y. Hong, C. Yu, J. Zhang, Q. Zhang, C.-Z. Peng, F. Xu, and J.-W. Pan, "Single-photon imaging over 200 km," Optica **8**, 344 (2021).
[13]E. Slenders, M. Castello, M. Buttafava, F. Villa, A. Tosi, L. Lanzanò, S. V. Koho, and G. Vicidomini, "Confocal-based fluorescence fluctuation spectroscopy with a SPAD array detector," Light: Sci. Appl. **10**, 31 (2021).
[14]C. Bruschini, H. Homulle, I. M. Antolovic, S. Burri, and E. Charbon, "Single-photon avalanche diode imagers in biophotonics: Review and outlook," Light: Sci. Appl. **8**, 87 (2019).
[15]N. Namekata, S. Adachi, and S. Inoue, "Ultra-low-noise sinusoidally gated avalanche photodiode for high-speed single-photon detection at telecommunication wavelengths," IEEE Photonics Technol. Lett. **22**, 529–531 (2010).
[16]K. Patel, J. Dynes, A. Sharpe, Z. Yuan, R. Penty, and A. Shields, "Gigacount/second photon detection with InGaAs avalanche photodiodes," Electron. Lett. **48**, 111 (2012).
[17]Y. Liang, E. Wu, X. Chen, M. Ren, Y. Jian, G. Wu, and H. Zeng, "Low-timing-jitter single-photon detection using 1-GHz sinusoidally gated InGaAs/InP avalanche photodiode," IEEE Photonics Technol. Lett. **23**, 887–889 (2011).
[18]A. Tosi, C. Scarcella, G. Boso, and F. Acerbi, "Gate-free InGaAs/InP single-photon detector working at up to 100 mcount/s," IEEE Photonics J. **5**, 6801308 (2013).
[19]Z. L. Yuan, B. E. Kardynal, A. W. Sharpe, and A. J. Shields, "High speed single photon detection in the near infrared," Appl. Phys. Lett. **91**, 041114 (2007).
[20]C. Scarcella, G. Boso, A. Ruggeri, and A. Tosi, "InGaAs/InP single-photon detector gated at 1.3 GHz with 1.5% afterpulsing," IEEE J. Sel. Top. Quantum Electron. **21**, 17–22 (2015).
[21]C. Park, S.-B. Cho, C.-Y. Park, S. Baek, and S.-K. Han, "Dual anode single-photon avalanche diode for high-speed and low-noise Geiger-mode operation," Opt. Express **27**, 18201–18209 (2019).
[22]Z. Lu, Y. Kang, C. Hu, Q. Zhou, H.-D. Liu, and J. C. Campbell, "Geiger-mode operation of Ge-on-Si avalanche photodiodes," IEEE J. Quantum Electron. **47**, 731–735 (2011).
[23]E. Amri, G. Boso, B. Korzh, and H. Zbinden, "Temporal jitter in free-running InGaAs/InP single-photon avalanche detectors," Opt. Lett. **41**(24), 5728–5731 (2016).
[24]A. C. Farrell, X. Meng, D. Ren, H. Kim, P. Senanayake, N. Y. Hsieh, Z. Rong, T.-Y. Chang, K. M. Azizur-Rahman, and D. L. Huffaker, "InGaAs–GaAs nanowire avalanche photodiodes toward single-photon detection in free-running mode," Nano Lett. **19**(1), 582–590 (2018).
[25]R. W. P. Drever, J. L. Hall, F. V. Kowalski, J. Hough, G. M. Ford, A. J. Munley, and H. Ward, "Laser phase and frequency stabilization using an optical resonator," Appl. Phys. B **31**, 97–105 (1983).
[26]K.-H. Luo, H. Herrmann, S. Krapick, B. Brecht, R. Ricken, V. Quiring, H. Suche, W. Sohler, and C. Silberhorn, "Direct generation of genuine single-longitudinal-mode narrowband photon pairs," New J. Phys. **17**, 073039 (2015).
[27]V. Ansari, E. Roccia, M. Santandrea, M. Doostdar, C. Eigner, L. Padberg, I. Gianani, M. Sbroscia, J. M. Donohue, L. Mancino, M. Barbieri, and C. Silberhorn, "Heralded generation of high-purity ultrashort single photons in programmable temporal shapes," Opt. Express **26**, 2764–2774 (2018).
[28]S. Signorini and L. Pavesi, "On-chip heralded single photon sources," AVS Quantum Sci. **2**, 041701 (2020).
[29]P. Sekatski, N. Sangouard, F. Bussières, C. Clausen, N. Gisin, and H. Zbinden, "Detector imperfections in photon-pair source characterization," J. Phys. B **45**, 124016 (2012).